21st Annual CFD Symposium, August 8-9, 2019, Bangalore

INVESTIGATIONS ON THE SHAPE OPTIMIZATION OF NACA0012 IN GROUND EFFECT

Dennis J[a], Chris J[a], Digin MB[a], Franklin J[a], Jithin PN[a], A. Viswanath[b], Ajith Kumar Arumugham-Achari[a]*
[a] Department of Mechanical Engineering, Rajagiri School of Engineering and Technology, Kochi, India
[b] Department of Civil Engineering, Rajagiri School of Engineering and Technology, Kochi, India
*Corresponding author email: ajithk@rajagiritech.edu.in

Abstract

A gradient based shape optimization was performed using the ANSYS® Adjoint Solver, on a symmetrical aerofoil (NACA0012) flying in proximity to ground, in order to improve its lift over drag ratio (*L/D*) at various heights and angles of attack in-ground-effect (IGE). The aerofoil profile optimization, with a fixed chord length and an unconstrained trailing edge, were aimed to augment *L/D* by at least 10%. Prior to shape optimization, SST k-ω turbulence model was chosen for the simulations, after its validation with existing literature for NACA0012 flying out-of-ground effect (OGE) at a Reynolds number of 3×10^6. The initial study also included investigations on the performance characteristics of the original aerofoil for IGE. Further, wind tunnel tests were performed using mirror image model technique, to check the suitability of the chosen turbulence model for IGE. For the original NACA0012 profile in ground proximity, venturi effect contributes to negative lift until an angle of attack of 5°, thereafter which *L/D* improves with higher angles of attack before reaching early stall (when compared with that of OGE). Comparison of the results of wind tunnel tests to simulations indicate close predictions in the values of coefficient of pressure (C_p) at lower angles of attack. However at higher angles of attack for IGE, we observe that the SST k-ω turbulence model fails to fully capture the flow separation and the resulting drop in C_p towards the leading edge of aerofoil, thereby over predicting *L/D* for such cases. This numerical delay in flow separation can be attributed mainly to the inaccuracy for turbulence dissipation rate (ω) modelled in the flow solver, which calls for caution in its use for such applications. On the other hand, Spalart-Allmaras was found to perform better than the shear stress transport model for the simulations of IGE at higher angles of attack. However, since the compatibility for ANSYS® Adjoint Solver is limited to variants of k-ω and k-ε turbulence models, we proceed with SST k-ω which is suitable for the present simulations at low angles of attack and IGE. Optimized shapes of an aerofoil in ground effect could be useful for applications such as Unmanned Aerial Vehicles (UAV) with morphing wing capabilities, seaplanes, or any engineering application which calls for adaptive aerofoil profiles operating near ground.

Keywords: Aerodynamics, Shape optimization, Ground effect, UAV, seaplanes, ANSYS® Adjoint Solver, NACA0012

Nomenclature

L = Lift (N)
D = Drag (N)
c = chord length (m)
C_L = coefficient of Lift
C_D= coefficient of drag
C_P= Coefficient of pressure
α = angle of attack (degrees)
h/c = height above ground to chord length

x/c = non-dimensional distance along the chord line
k = turbulent kinetic energy (m^2/s^2)
ε = rate of dissipation of turbulence energy (m^2/s^3)
ω = specific rate of dissipation of k (s^{-1})
μ = dynamic viscosity (Pa.s)
$\bar{u}, \bar{v}, \bar{w}, \bar{P}, \bar{\rho}$ = time averaged velocity components in x, y, z directions (m/s), pressure (N/m^2) and density (kg/m^3) respectively
$\bar{U}$ = time averaged free stream velocity (m/s).
$\overline{u'}, \overline{v'}, \overline{w'}$ = fluctuating components of velocity in x, y and z directions respectively (m/s)
μ_T = turbulent viscosity (m^2/s)
P_k = rate of production of turbulent kinetic energy (m^2/s^3)
$\beta_2, \sigma_{\omega 1}, \sigma_{\omega 2}, \sigma_k, \gamma_2, \beta_*$ = model constants for SST k-ω turbulence model
δ_{ij} = kronecker delta
S_{ij} = mean rate of strain considering x and y direction
CFD = Computational Fluid Dynamics
F_x,F_y, F_z= body force per unit volume acting along x, y, $z$directions respectively (N/m^3)

1. Introduction

Excessive dependence on fossil fuels for aviation has led researchers to improve lift over the drag ratio (*L/D*) of aircraft wings, since the aircraft engine efficiency is directly related to *L/D* through Breguet formula. This calls for either redesigning or economically viable modifications of the original wing profile. With advancements in computational resources, shape optimization for the aircraft wing has become a very reliable course of action for achieving the same. Also considered has been the use of seaplanes, which operate in close proximity to sea surface, thereby enhancing the lift to drag ratio compared to a plane flying out of the ground. Ram effect experienced by wings flying close to the ground, in addition to a reduction in induced drag experienced by such planes, allow them to be much more efficient compared to conventional aircrafts. At the same time they are faster than sea vessels.

Shape optimization through various methods has been discussed in several computational works on aerodynamic structures. Namgoong et al. [1] on comparing gradient-based optimization to the genetic-based optimization for a morphing aerofoil explains that while gradient-based algorithm gives a local minimum, genetic algorithm gives a global minimum. However, multi-objective optimization is easier and computationally less expensive in gradient based optimization compared to the latter.

Ahmed et al. [2] experimentally studied the flow characteristics over a symmetrical aerofoil (NACA0015). From the experiments conducted in a low-speed wind-tunnel it was found that both the angle of attack and the ground clearance have a strong influence on the aerodynamic characteristics of the aerofoil. Lift coefficients obtained from integrating surface pressure distribution and from direct load cell measurements showed that as *h/c* reduces, the sign of lift coefficient remains unchanged but its magnitude increases. However, a strong suction effect is observed on the lower surface of the aerofoil at certain ground clearances at angles of attack up to 5^o, which he attributes to the venturi effect resulting from the formation of a convergent divergent passage between the symmetrical aerofoil and the ground in close proximity.

CFD and PIV based studies were performed by Barber et al. [3] to investigate the various influences of ground effect, and they found that a '*moving ground*' is the only accurate ground boundary condition for body-fixed simulation. They also observed that flow separation over an aerofoil occurs at angles of attack earlier than for a wing in free air.

Kyoungwoo et al. [4] made use of a gradient-based optimization process to optimize the shape of a wing in ground effect, in which the static height stability and the negative moment coefficient were used for defining the stopping criteria. Their work indicates that while a flatter lower surface is expected to enhance the cushioning effect experienced by a wing in ground effect, a true symmetrical aerofoil is unfit to be used in ground proximity as the values for its static height stability are larger than zero.

The influence of a flap on the two dimensional NACA4412 aerofoil in viscous ground effect flow was numerically investigated by Alex et al. [5]. With the addition of a flap in extreme ground proximity, the effects of flap deflection, ground height, flap type, angle of attack, and Reynolds number were studied. As the flap is deflected, the flow is trapped beneath the aerofoil, leading to decrease of flow velocities and build-up the pressure below the aerofoil. Drag coefficient was found to significantly increase as the flap is deflected.

The shape optimization of the two-dimensional wing in ground effect (WIG) has been performed by the integration of CFD and MOGA (Multi-Objective Genetic Algorithm) by Juhee et al. [6]. From the analysis of these Pareto optima, which included the various aerofoil shapes, they found that the relation between C_L and C_L/C_D is linearly dependent but the other two relationships, between height stability and C_L and between height stability and C_L/C_D, are not.

For the comparison of trends of turbulence model in ANSYS® Fluent, Eleni et al. [7] compared the wind tunnel values obtained by Abbott et al. [8] to those obtained with different turbulence models available in Fluent. The SST k-ω turbulence model predicted values closest to those obtained by Abbott et al. [8]. The errors in predicting the coefficient of drag was attributed mainly due to the failure of turbulence models in calculating the transition point from laminar to turbulent and the model's consideration that the boundary layer is turbulent throughout its length.

Parviz et al. [9] examined the aerodynamic characteristics of various symmetrical aerofoils such as NACA0009, NACA0012, NACA0015, and NACA0018. For these symmetrical aerofoils at very low flight altitude, and at low angles of attack, the lift force was found to decrease while the drag increased with respect to increasing thickness of the aerofoil. They reasoned that the establishment of a converging-diverging passage at the lower surface could have caused the above phenomena. For a larger angle of attack when approaching the ground surface, the transition phenomenon moved towards the trailing edge. This concludes that approaching ground surface causes local Reynolds number to decrease, which in turn delays transition.

Studies on the flow over an aerofoil in ground proximity have been limited due to difficulty in carrying out such experiments and simulations. However, studies conducted so far, such as that by Wang Hao et al. [10], have been able to closely observe the now well-known suction effect and ram effect in ground proximity. While investigating the range of heights and pitch angles of NACA4412, they explain that the Aerodynamic Centre of Height (ACH) for an aerofoil is only a function of pitch angle, while Aerodynamic Centre with respect to pitch (ACP) is only a function of height. And also, that the ACH for NACA4412 lies behind the ACP. When viscous effects are taken into account, the ACH of the NACA4412 aerofoil moved further forwards due to boundary layer de-cambering effects.

An 'Adjoint Solver' is a post-processing tool provided in ANSYS® Fluent that extends the analysis of a conventional flow solver by giving detailed sensitivity data for the performance of a fluid system. This sensitivity data obtained can be for any observable such as lift, drag and pressure drop etc., based on the engineering quantity of interest. This sensitivity data obtained can be useful for a number of reasons. In a fluid system such as a duct, that is highly sensitive may exhibit improved performance due to small variations in manufacturing or changes in the surrounding flow environment in which it is operating. Alternatively, it also shows us that the device under study can still be improved so as to improve its efficiency.

Muñoz et al. [11] used the Adjoint Solver in ANSYS® Fluent to optimize the shape of the nose of a bullet train by constraining its nose length according to European Standards. Six iterations were required to reach an optimized shape and the stopping criteria used by the authors was the volume required for the end coupler and the crash structure. Zhang et al. [12] provided a novel method to optimize the fin of a heat exchanger by increasing the heat transfer and decreasing the drag encountered by it, by varying four geometric properties, specifically the pitch, length, width and height within a specified range. Although the change produced was not as prominent, the multi-objective optimization process ended up with a decrease in drag and increase in heat transfer.

In the present work, we envisage to attain a harmonious blend of all the concepts mentioned above. Investigations on the optimum shapes for a symmetric aerofoil in proximity to ground has been carried out, under various heights above ground and at various angles of attack. A symmetric aerofoil (NACA0012) was selected, for it offers no lift at zero angle of attack. Also large data is available for validation for OGE. Hence for a meaningful comparison in study. For the shape optimization, we have employed Adjoint Solver module in ANSYS® Fluent, which worked in association with the most suitable SST k-ω turbulence model in the flow solver. Such investigations could lead to developing morphing wings, for example of an unmanned surveillance aircraft. Radar evasion and endurance could be the salient features of it.

2. Governing Equations

2.1 SST k-ω Turbulence model:

This hybrid turbulence model uses k-ε model for regions far from the wall and a k-ω model near wall regions. The full set of the governing equations of the turbulence model are given below

Continuity Equation:

$$\frac{\partial\bar{\rho}}{\partial t}+\frac{\partial\bar{u}}{\partial x}+\frac{\partial\bar{v}}{\partial y}+\frac{\partial\bar{w}}{\partial z}=0 \tag{1}$$

Momentum (Reynolds Averaged Navier Stokes) Equations:

$$\bar{\rho}\left(\frac{\partial\bar{u}}{\partial t}+\bar{u}\frac{\partial\bar{u}}{\partial x}+\bar{v}\frac{\partial\bar{u}}{\partial y}+\bar{w}\frac{\partial\bar{u}}{\partial z}\right)=-\frac{\partial\bar{p}}{\partial x}+\mu\Delta\bar{u}-\bar{\rho}\left(\frac{\partial\overline{u'u'}}{\partial x}+\frac{\partial\overline{u'v'}}{\partial y}+\frac{\partial\overline{u'w'}}{\partial z}\right)+F_x \tag{2}$$

$$\bar{\rho}\left(\frac{\partial\bar{v}}{\partial t}+\bar{u}\frac{\partial\bar{v}}{\partial x}+\bar{v}\frac{\partial\bar{v}}{\partial y}+\bar{w}\frac{\partial\bar{v}}{\partial z}\right)=-\frac{\partial\bar{p}}{\partial y}+\mu\Delta\bar{v}-\bar{\rho}\left(\frac{\partial\overline{v'u'}}{\partial x}+\frac{\partial\overline{v'v'}}{\partial y}+\frac{\partial\overline{v'w'}}{\partial z}\right)+F_y \tag{3}$$

$$\bar{\rho}\left(\frac{\partial\bar{w}}{\partial t}+\bar{u}\frac{\partial\bar{w}}{\partial x}+\bar{v}\frac{\partial\bar{w}}{\partial y}+\bar{w}\frac{\partial\bar{w}}{\partial z}\right)=-\frac{\partial\bar{p}}{\partial z}+\mu\Delta\bar{w}-\bar{\rho}\left(\frac{\partial\overline{w'u'}}{\partial x}+\frac{\partial\overline{w'v'}}{\partial y}+\frac{\partial\overline{w'w'}}{\partial z}\right)+F_z \tag{4}$$

Transport equations for k and ω:

$$\frac{\partial(\rho k)}{\partial t}+\nabla\cdot(\rho kU)=\nabla\cdot\left(\left(\mu+\frac{\mu_t}{\sigma_k}\right)\nabla(k)\right)+P_k-\beta^*\rho k\omega \tag{5}$$

$$\frac{\partial(\rho\omega)}{\partial t}+\nabla\cdot(\rho\omega U)=\nabla\cdot\left(\left(\mu+\frac{\mu_t}{\sigma_\omega}\right)\nabla(\omega)\right)+\gamma_2\left(2\rho S_{ij}.S_{ij}-\frac{2}{3}\rho\omega\frac{\partial U_i}{\partial x_j}\delta_{ij}\right)-\beta_1\rho\omega^2+2\frac{\rho}{\sigma_{\omega,2}\omega}\frac{\partial k}{\partial x_k}\frac{\partial\omega}{\partial x_k} \tag{6}$$

2.2 Adjoint solver and the key ideas

Let J be the engineering quantity of interest for the optimization. Then

$$J=J\left(\underline{q},\underline{c}\right) \tag{7}$$

where $\underline{q}$ represents the flow solution and $\underline{c}$ the inputs to the problem. After obtaining the flow solution, due to convergence, the residuals of the Navier-Stokes equations, $\underline{R}$ should ideally be zero, *i.e*,

$$\underline{R}\left(\underline{q},\underline{c}\right)=0 \tag{8}$$

Changing the problem definition slightly, by changing an input $\underline{c}$ by $\delta\underline{c}$, this changes the output quantity J by δJ

$$\delta J=\frac{\partial J}{\partial\underline{q}}\,\delta\underline{q}+\frac{\partial J}{\partial\underline{c}}\,\delta\underline{c} \tag{9}$$

This involves a change in the flow. But the interest lies only in changes in the output quantity. Thus to eliminate the change in the flow, consider that the change in input leads to a change in output, and linearize the Navier-Stokes equation.

$$\frac{\partial R}{\partial\underline{q}}\,\delta\underline{q}+\frac{\partial R}{\partial\underline{c}}\,\delta\underline{c}=0 \tag{10}$$

Thus, a relationship can be established between the variations in the flow to that of the input by engineering a particular linear combination of linearized Navier Stokes Equations by introducing multipliers $\underline{\tilde{q}}$ as shown in equation (11).

$$\left(\left(\underline{\tilde{q}}\right)^T\frac{\partial R}{\partial\underline{q}}\right)\delta\underline{q}+\left(\underline{\tilde{q}}\right)^T\frac{\partial R}{\partial\underline{c}}\delta\underline{c}=0 \tag{11}$$

The left term on the left hand side is used to formulate the adjoint equations to be solved by equating it with the change in the output quantity with respect to the flow solution $\underline{q}$, as shown in equation (12).

$$\left\{\frac{\partial \underline{R}}{\partial \underline{q}}\right\}^T \underline{\tilde{q}} = \frac{\partial J}{\partial \underline{q}} \tag{12}$$

Using this the above relationship can be used to determine the change in the engineering quantity w.r.t the input variables alone, that is,

$$\delta J = \left\{\frac{\partial J}{\partial \underline{c}} - \underline{\tilde{q}}^T \frac{\partial \underline{R}}{\partial \underline{c}}\right\} \delta \underline{c} \tag{13}$$

Thus, by solving equation (12), we obtain equation (13), an equation relating the change in the output quantity of interest with respect to inputs to the flow problem. This gives the sensitivity data based on which the optimization occurs.

3. Methodology

3.1 Verification and Validation of Numerical schemes

In order to select the appropriate turbulence model for the simulations of OGE (to be chosen from SST k-ω, Realizable k-ε, Standard k-ε and Spalart-Allmaras turbulence models), verification was necessary with respect to the results from wind tunnel tests of a NACA0012 flying *'out of ground effect'* conditions. These comparisons were made based on the experimental results of Abbott et al. [8] at a Reynolds number of 3×10^6. These simulations were carried out on a C-topology grid created in ICEM CFD® (Fig. 1). Based on the calculations, a y^+ value of 1.77 was used to determine the first cell height.

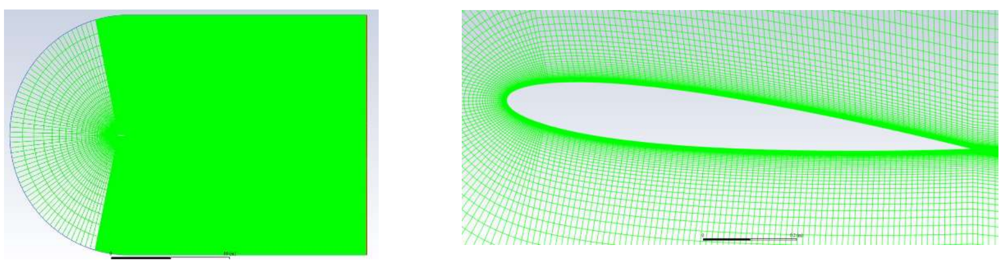

Fig. 1. The C-topology grid for verification procedure with $y^+ = 1.77$

The boundary conditions used for the simulations were as follows. Inlet velocity of 45 m/s was given in the horizontal direction towards the aerofoil, and the outlet condition was given as atmospheric pressure. The aerofoil was given a no-slip condition. The coefficient of lift and coefficient of drag for the different turbulence models in Fluent® were recorded, plotted and compared with Abbott et al. [8] (Refer Fig. 2).

Though the coefficient of lift agrees closely with experimental results, there is a slight difference between the results obtained from the simulations and the wind-tunnel test when it comes to the coefficient of drag (Fig. 3). However, our simulations agree to the results obtained by Eleni et al. [7], who also pointed out to this discrepancy in predicting drag with turbulence models. He attributed this error with turbulence models considering the whole flow around the aerofoil as being turbulent, whereas in actual case a transition region exists, thus splitting the region into laminar and turbulent. This explains the reason for the slight overshoot in the estimate for drag coefficient.

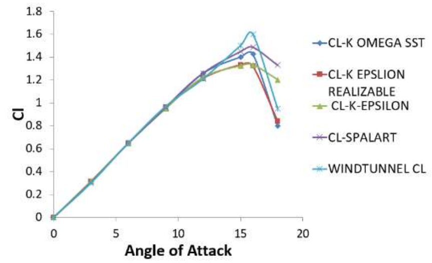

Fig. 2. Variation of C_L with α at $Re = 3\times10^6$

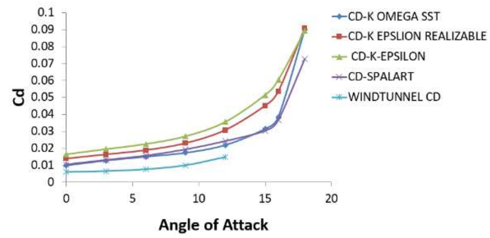

Fig. 3. Variation of C_D with α at $Re = 3\times10^6$

3.2 Validation of the usage of the Adjoint Solver

Cases that made use of the Adjoint Solver for the optimization of an aerofoil were scarce. Matthias et al. [13] made use of an Adjoint based optimization technique with an Adjoint turbulence model instead of a frozen turbulence model as used in the Adjoint Solver in ANSYS®. A computational domain and boundary conditions similar to that discussed in Section *3.1* was used for the present simulations too, the only difference being the $y+$ value was fixed to 0.1 as that of Matthias et al. [13], and the simulations were performed at a Reynolds number of 2×10^6.

As SST k-ω turbulence model showed closer values compared to wind-tunnel tests conducted by Abbott et al. [8], it was selected instead of the k-ε turbulence model. In cases involving turbulence, only these two turbulence models are compatible with the Adjoint Solver in ANSYS Fluent®. Matthias et al. [13] had used the Spalart-Allmaras turbulence model to conduct simulations with a flow solver using the Adjoint approach in OpenFOAM®. He had performed the shape optimization of a NACA0012 aerofoil at $\alpha = 2^o$ at OGE conditions to increase the lift by 20 percent. We performed similar OGE simulations with Adjoint Solver in ANSYS Fluent® and compared our results to that of Matthias et al. [13] to verify our simulations with shape optimization. The bounding box defined for the control volume meshing tool is shown in Fig. 4. The control points serve as anchor points for the mesh during morphing such that a displacement of a control point moves the local mesh with it. The smaller the spatial scale on which mesh changes on the order of 20 to 40 control points for each coordinate direction is typical. Displacement of point will not occur in regions of the shape that intersect the bounding box. The trailing edge was fixed by intersecting the bounding box required for the control volume meshing tool with the trailing edge of the aerofoil at $\alpha = 2^o$. This will allow us to fix the trailing edge of the aerofoil, similar to what Matthias had done. 30 control points were used along x direction, thus fixing the number of control points along y direction as 18.

The Adjoint equations for the lift force experienced by the aerofoil were solved and the sensitivity information with respect to lift was obtained. A 20% increase in the lift was targeted and the geometry was modified successfully. Results of the simulation are shown in Fig. 5. The optimized profile is close to that obtained by Matthias et al. [13].

Fig. 4. Bounding box defined for the control volume morphing tool. Note the bounding box fixing the trailing edge.

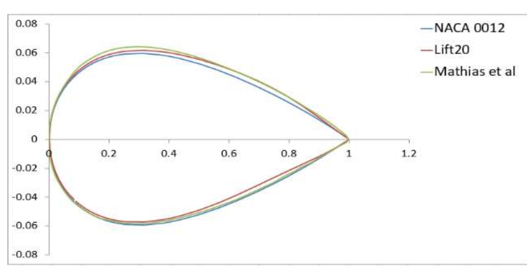

Fig. 5. Comparison of the shape optimized for 20% increase in lift

The slight quantitative differences between our simulations with that of Matthias can be attributed to the fact that ANSYS Fluent® has a discrete Adjoint solver with frozen turbulence assumption, whereas the simulations conducted by Matthias et al. [13] had a continuous Adjoint approach in OpenFOAM®, along with the adjoints to the Spalart-Allmaras turbulence model. Note that both the codes made use of adjoint-based equations to obtain the sensitivity information of the aerofoil for lift. Both these shapes show us that the areas predicted sensitive to the lift force are the same in both cases, although the displacement of the control points may vary.

3.3 Performance of unaltered NACA0012 in ground proximity

After a suitable turbulence model was selected as discussed in the previous sections, analysis of *L/D* was carried out for the original NACA 0012 profile in ground proximity. 36 different combinatorial simulations were carried out with SST *k-ω* turbulence model of ANSYS Fluent® at a Reynolds number of 2×10^6. The mesh was created in ICEM CFD with a $y+$ value of 1.1742. The boundary conditions used for the simulation, and a close look of the mesh near the aerofoil are given in Fig. 6 and 7 respectively.

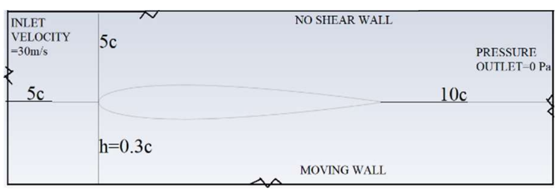

Fig. 6. Symmetric aerofoil close to the ground, along with the Boundary conditions (not to scale)

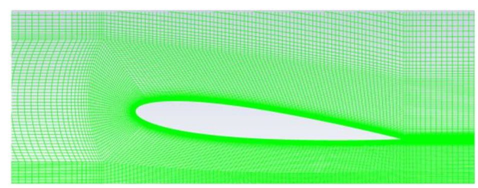

Fig. 7. Close up of the mesh: h/c = 0.3, α =4°

In Fig. 6, the distance of the aerofoil from the bottom wall is varied for the study in order to simulate conditions of aerofoil approaching ground proximity. The inlet flow velocity was fixed at 30 m/s. The bottom wall is provided with a '*moving wall*' boundary condition, which according to Barber et al. [3], is the only accurate ground boundary condition for body-fixed simulation and is given the same velocity as that at the inlet. The top domain wall is given a '*no specified shear*' condition and the exit section is given zero gauge pressure. The residuals were fixed to 10^{-4}. Similar meshes were recreated at different angles of attack to plot the variations with respect to the angle of attack. The fluid has a fluid density of 1.225 $\mathrm{kg/m^3}$ and dynamic viscosity of 1.7894×10^{-5} Pa s. Mesh dependency tests were conducted to recognize the ideal number of nodes required to give accurate results at reduced computational cost. The value of the coefficient of lift became steady when number of nodes were greater than 340000. Thus 345072 nodes were used for the further simulations. The results obtained were compared with that of wind tunnel tests as discussed below.

3.4 Wind-tunnel experiments

For the validation of simulations conducted In Ground Effect (IGE) conditions, it was necessary to perform wind tunnel tests and compare the results to those obtained by the simulations. This will help to select a turbulence model most suitable to simulate IGE conditions. This validation was performed by comparing the plots for coefficient of pressure with that obtained from wind tunnel tests conducted at the Subsonic Wind Tunnel Test Facility, Viswajyothi College of Engineering and Technology, Kerala (Fig. 8). The mirror image model technique was used to simulate the flight of NACA0012 aerofoil in ground proximity (Fig. 9).

Pressure ports were provided along the upper and lower surfaces of the NACA0012 aerofoil. These pressure ports were connected to an alcohol based manometer. Pitot static tubes were provided inside the test section of wind tunnel for measuring the static and stagnation pressures of the ambient flow. To study the effect of ground on the flow modifications, the ground must be having no relative velocity with respect to the ambient air. But with a model fixed in the test section of the wind tunnel, boundary layer developing over the wind tunnel test section can affect the flow characteristics. Therefore, to simulate a '*moving ground*' which has no relative velocity with respect to incoming airflow, Mirror image model technique was used. This method consists of having two aerofoils kept at suitable heights such that the moving ground will be the imaginary midplane at an equidistant height from both aerofoils. For *eg.*, two NACA0012 aerofoils were placed at a distance of 7 cm from each other to create a ground plane at exactly 3.5 cm distant relative to either aerofoils. Static pressure measurements can be deduced from either one of the aerofoils.

Fig. 8. Wind Tunnel test facility

Fig. 9. Mirror image model technique

3.5 Shape optimization of the symmetric aerofoil in ground proximity

Using the Adjoint Solver, optimized shapes were obtained for NACA0012 aerofoil in ground proximity by the following steps as shown in the flowchart (Fig. 10). Four meshes were created of NACA0012 aerofoil at a height of 1/5th of the chord length from the ground, at various angles of attack, *viz.*, 2^o, 4^o, 6^o and 8^o. A $y+$ value of 1.1742 was used for the meshes as it was noticed that the Adjoint equations had convergence issues at very low $y+$ values (for e.g., with $y+= 0.1$). The mesh consisted of a rectangular computational domain, similar to the ones used for the study of NACA0012 in ground proximity (Fig. 6). After solving the Adjoint equations, the sensitivity of the observable was calculated and was used for optimization using the control volume meshing tool.

The size of the bounding box used for the optimization was defined using the '*comfortable region'* option (Fig. 11). This option automatically selects a bounding box about the region to be optimized such that mesh continuity is not disturbed within and outside the control volume selected. Although it selects the box as said, the distance from the leading edge was set to zero so as to fix the leading edge of the aerofoil, as is done in most morphing wing applications. The bounding box finally decided is as given in Fig. 11. The motion of the control points along y-direction was the only interest. Twenty control points were defined along the y-direction. Motion along the x-direction was disabled. The optimization was based on a target change in the quantity of the observable. Going for a large target change can lead to a reduction in mesh quality. Thus, only 10% improvement in the *L/D* ratio is targeted for the present optimization studies.

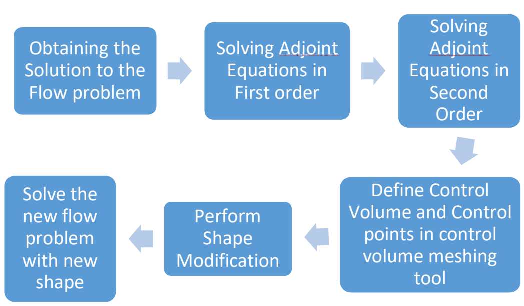

Fig. 10. Steps for optimization using the Adjoint Solver

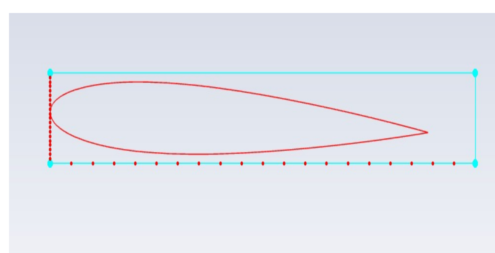

Fig. 11. Bounding box defined for optimization

4. Results and Discussions

Through the various simulations, we initially determined the extent of ground effect a symmetrical airfoil experiences in ground proximity, by plotting the C_L vs h/c at α = 0° configuration (Refer Fig. 12). Further simulations were carried out by varying angles of attack and height above ground (Refer Fig. 13). The variation of lift to drag ratio in such combinations were also plotted as C_L/C_D vs. h/c (Refer Fig. 14). From these results, we observe that at low angles of attack ($\alpha \leq 3°$) when near ground, a strong suction effect is experienced that tends to decrease the overall lift experienced by the aerofoil. This is due to the converging-diverging shape created between the ground and lower surface of the symmetrical aerofoil, that tends to accelerate the flow in this lower region thus leading to a low-pressure zone ('*venturi effect*') that tends to decrease the overall lift. This phenomenon can be clearly observed in Fig. 12, with α = 0° configuration for which a sharp negative lift is observed IGE. However, at higher angles of attack, the ground effect is different from the former (Refer Fig. 13). By α = 4°, both suction effect and ram effect are observed to affect the lift equally. Ram effect contributes to high pressure at the lower surface of the aerofoil. For larger angles of attack, the lift over drag ratio is observed to increase as we move closer to ground proximity. The larger values of C_L/C_D is observed about an α = 8° and it decreases thereafter at higher angles, due to the early onset of stall condition. In Fig. 14, at h/c = 0.5, the coefficient of lift is indicates that the aerofoil has moved into the zone of OGE. Thus, we can conclude that a original unaltered NACA0012 profile experiences ground effect for $h/c \leq 0.5$.

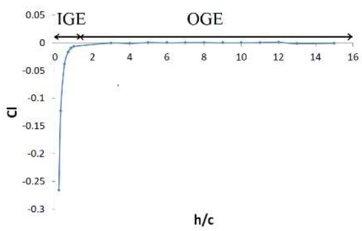

Fig. 12. C_L vs. h/c for at α =0°

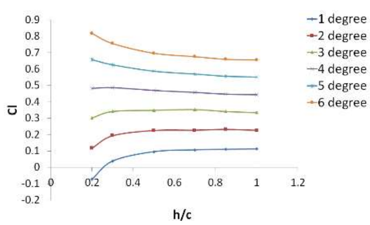

Fig. 13. Coefficient of lift vs h/c for NACA0012 at various angles of attack

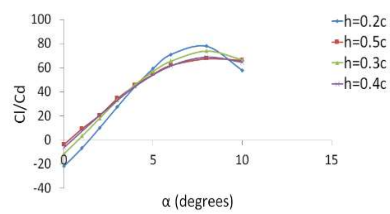

Fig. 14. Coefficient of lift over drag vs Angle of Attack at various h/c

The results of simulations for the unaltered original NACA0012 under IGE with various turbulence models were compared with that of the results of the wind-tunnel tests using Mirror image model technique. The choice of turbulence model suitable to simulate IGE for further shape optimized profiles from NACA0012 were based on these results. We found that at lower angles of attack ($\alpha \leq 10°$), pressure distributions obtained from experiments were close to that predicted by the various turbulence models of ANSYS Fluent® (Figs. 15 (a, b, c)). However, there is major difference in the prediction of pressure distribution over upper surface of aerofoil at higher angles of attack ($\alpha > 10°$) (Refer Fig. 15 (d)).

The wall jet flow between the lower surface of the aerofoil and the ground, is suddenly exposed to a flow of different momentum above the upper surface of the aerofoil, as soon as it reaches the trailing edge. This chaotic mixing in the actual flow physics may not be effectively captured by the turbulence models. SST k-ω has been known for its weakness for over predicting turbulence dissipation rate ε, similar to the shortcoming of k- ε model [14]. Over predicting turbulence dissipation rate can introduce artificial turbulence in flow separation regions, thereby failing to capture early stalling associated with high angles of attack under IGE. This can be clearly observed in Fig. 15 (d), that only at higher angles of attack with IGE condition (h/c = 0.35) the prediction of pressure distribution on the upper surface is quite different from that obtained through the wind-tunnel tests.

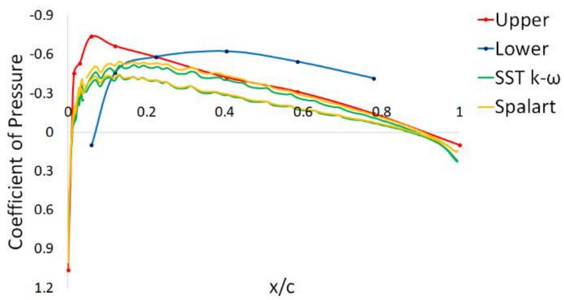

(a) α =0º

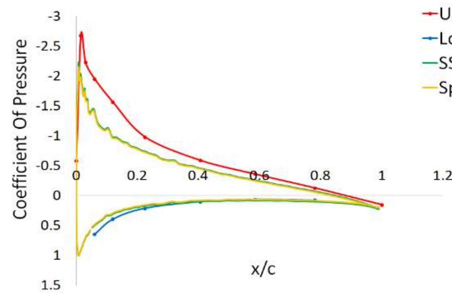

(b) α =5 º

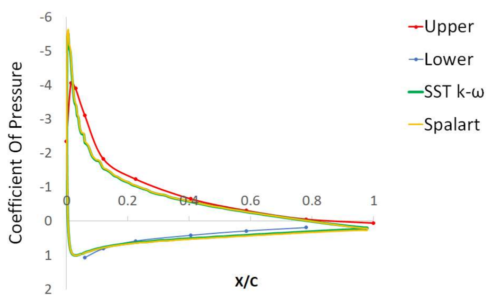

(c) α =10º

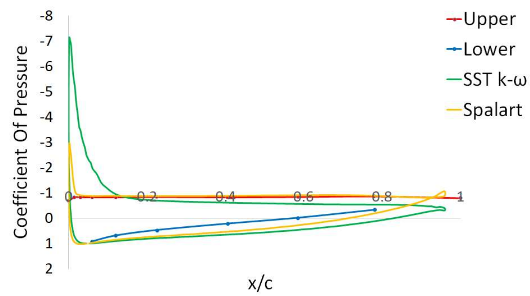

(d) α =15º

Fig. 15. Variation of C_P with α for IGE at h/c = 0.35: Comparison of SST k-ω and Spalart Allmaras turbulence models with respect to wind tunnel experiments

However, at lower angles of attack, both the SST k-ω and the Spalart-Allmaras turbulence model shows good prediction when compared to the experimental results. It should also be noted that higher angles of attack, the Spalart-Allmaras turbulence model performs better. However, Spalart-Allmaras turbulence model is not available for the Adjoint Solver in ANSYS Fluent®. Also, with the early onset of stall condition for IGE and aiming only for 10% increase in L/D, it is sufficiently correct to proceed with SST k-ω for the present shape optimization simulations on NACA0012, which were basically carried out at lower angles of attack ($\alpha \leq 8^{o}$).

For h/c = 0.2 IGE at α = 2º, 10% increase in the L/D ratio was easily achieved, with the camber line variations occurring most strongly near the trailing edge (Fig. 16 (a)). Similar trend is observed with the case of α = 4º, where the trailing edge is also the main region for modification, along with an appreciable modification to the lower surface (Fig. 16 (b)). However, at α = 6º, the final objective value (actual gain in L/D of 5% only) obtained is different from that desirable value initially targeted by the solver (desirable gain in L/D of 10%) (Refer Fig. 17 (a)). This similar trend is continued to be observed at α = 8º (Fig. 17 (b)). This is primarily because of the frozen turbulence assumption implemented in the ANSYS® Adjoint solver, that results to its poor optimization performance at higher angles of attack. Under this assumption, the effect of changes to the state of the turbulence is not taken into account when computing sensitivities. Thus, one should be cautious while using this optimization solver to achieve increase in the L/D ratio for higher angles of attack with IGE. However, under such condition a sufficiently accurate optimized profile, though with lesser gain in L/D is obtained, and has been verified by us through stand alone simulations performed on such optimized shapes generated.

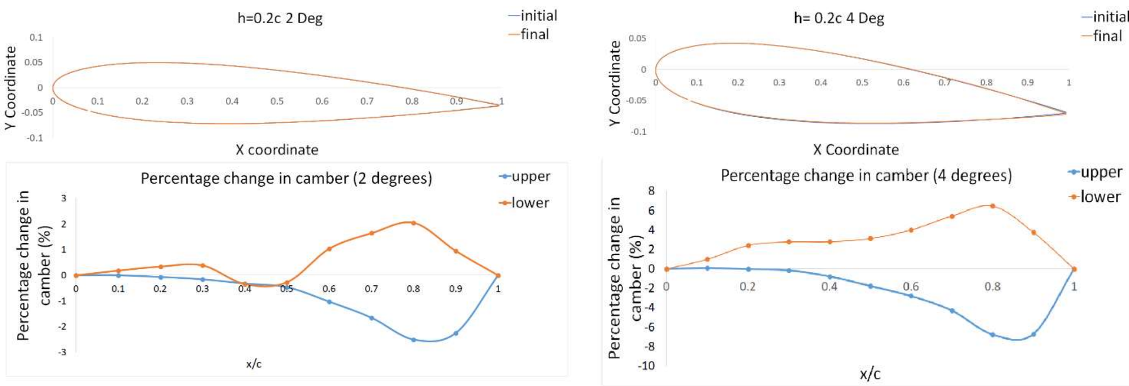

(a) h/c = 0.2 at α =2°
Initial L/D = 12.05583;
Expected change as per solver = +1.20583
Final obtained L/D = 13.19764

(b) h/c = 0.2 at α =4°
Initial L/D = 47.69205;
Expected change as per solver = +4.769205
Final obtained L/D = 51.55728

Fig. 16. Initial and final obtained L/D using Adjoint solver **for low angles of attack**, with optimized final shape represented as percentage change in camber

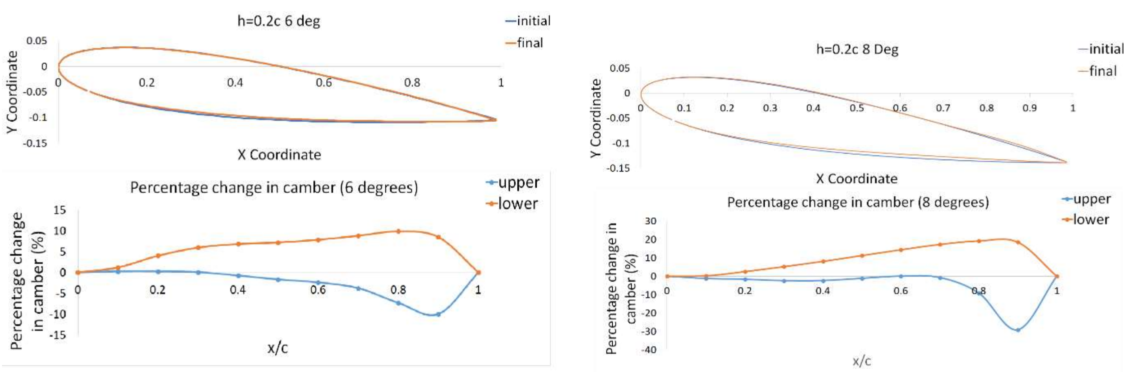

(a) h/c = 0.2 at α =6°
Initial L/D = 77.05747;
Expected change as per solver = +7.705747
Final obtained L/D = 81.0866592

(b) h/c = 0.2 at α =8°
Initial L/D = 87.199072;
Expected change as per solver = +8.7199072
Final obtained L/D = 91.635925

Fig. 17. Initial and final obtained L/D using Adjoint solver **for higher angles of attack**, with optimized final shape represented as percentage change in camber

5. Conclusion

A gradient based optimization using ANSYS® Adjoint solver was performed on a NACA0012 aerofoil in ground proximity to optimize the its shape and achieve improved lift over drag ratio, at various heights near ground. When comparing the simulations to the wind tunnel tests of Abbott et al. [8], it was observed that the SST k-ω turbulence model showed better results close to that of the wind tunnel test compared to other turbulence models conducted at in OGE condition. Studies of NACA0012 aerofoil in ground proximity using simulations conducted in ANSYS® Fluent suggested that the ram effect which causes lift augmentation when moving in ground proximity starts only at α greater than 4 degrees. The suction effect is predominant for $\alpha \leq 4°$.

To validate the simulations conducted in ground proximity, wind-tunnel tests were carried out using mirror image model technique. Close predictions were made at lower angles of attack. However, the SST k-ω turbulence model performed poorly when compared to Spalart-Allmaras turbulence model in predicting the early stall associated with the IGE at higher angles of attack. Since our studies were performed in comparatively lower angles of attack ($\alpha \leq 8^o$, due to early stalling IGE), ANSYS® Adjoint Solver compliant with SST k-ω turbulence model was used in our simulations. The optimized shapes at different ground proximities and at various angles of attack, to augment lift over drag ratio by about 10% were obtained while constraining the leading edge of the aerofoil. However, at higher angles of attack, the desirable lift augmentation of 10% could not be achieved using the Adjoint solver, due to the frozen turbulence assumption implemented in the same. (But one can make use of an Adjoint turbulence assumption and generate shapes with their own code to get improved shapes at higher angles of attack). These optimized shapes obtained will be useful for applications like intelligent UAV, surveillance seaplanes etc. with morphing wing capabilities. The longitudinal stability of these shapes in ground proximity which has not been answered in the present work, will be studied in the near future.

Acknowledgement

This work has been carried out as a part of the 'Morphing wings' project of the Computer Aided Engineering (CAE) Research Group of the Department of Mechanical Engineering at Rajagiri School of Engineering and Technology, Kochi. Valuable suggestions and help offered by the other team members of the project group is gratefully acknowledged. We express our sincere gratitude to Prof. (Retd.) K.J Devasia, for his valuable guidance and suggestions in conducting experiments for this study. Thanks to Mr. Vinoj K, and Mr. Benny Sebastian of the Department of Mechanical Engineering, Viswajyothi School of Engineering and Technology, Kerala for extending to us the wind tunnel facility of their institution.

References

1. Howoong Namgoong.2005. “Airfoil optimization for morphing aircraft”. Ph.D. Thesis, Purdue University
2. M.R. Ahmed A and S.D. Sharma. 2005. “An investigation on the aerodynamics of a symmetrical aerofoil in ground effect”. *Experimental Thermal and Fluid Science* 29 (6): pp. 633-647.
3. Tracie J. Barber and Stephen Hall. 2006. “Aerodynamic ground effect: A case study of the integration of CFD and experiments”. *International Journal of Vehicle Design* 40(4).
4. Kyoungwoo Park, Byeong Sam Kim, Juhee Lee and Kwang Soo Kim. 2009. “Aerodynamics and Optimization of Airfoil”. *International Journal of Aerospace and Mechanical Engineering* 3 (4).
5. Alex E.Ockfen and Konstantin I. Matveev. 2009. “Aerodynamic characteristics of NACA4412 airfoil section with flap in extreme ground effect”. *International Journal of Naval Architecture and Ocean Engineering* 1 (1): pp. 1-12.
6. Kyoungwoo Park and Juhee Lee. 2010. “Optimal design of two-dimensional wings in ground effect using multi-objective genetic algorithm” *Ocean Engineering* 37(10): pp. 902–912.
7. Eleni Douvi, Tsavalos I Athanasios and Dionissios P. Margaris. 2012. “Evaluation of the turbulence models for the simulation of the flow over a National Advisory Committee for Aeronautics (NACA) 0012 airfoil”. *Journal of Mechanical Engineering* 4 (3): pp. 100-111.
8. Ira H. Abbott and Albert E. von. 1959. “*Theory of Wind Sections: Including a Summary of Airfoil Data*”. Dover Publications, INC. New York.
9. Parviz Ghadimi, Ali Bakhshandeh Rostami, Farzad Jafarkazemi. 2013. “Aerodynamic analysis of the boundary layer region of symmetric”. *Aerospace Science and Technology* 17 (1): pp. 7-20.
10. Wang Hao, CJ Teo, BC Khoo and CJ Goh.2013. "Aerodynamic and stability characteristics of NACA4412 in ground effects". *International Journal of Intelligent Unmanned Systems* 1 (2): pp. 145-153.
11. J. Muñoz-Paniagua, Javier Garcia and Antonio Crespo. 2015. “Aerodynamic Optimization of the Nose Shape of a Train Using the Adjoint Method”. *Journal of Applied Fluid Mechanics*8 (3): pp. 601-612.

12. Cheng-Zhang Wang, Kondala Rao Nagisetty, Federico Montanari and D. Chris Hill. 2015. “Application of Adjoint Solver to Optimization of Fin Heat Exchanger”. *ASME Turbo Expo 2015: Turbine Technical Conference and Exposition*.
13. Matthias Schramm, Bernhard Stoevesandt and Joachim Peinke. 2018. “Optimization of Aerofoils Using the Adjoint Approach and the Influence of Adjoint Turbulent Viscosity”. *Computation 2018* 6 (5).
14. H.K. Versteeg and W.Malalasekera,2017, "*An Introduction to Computational Fluid Dynamics. The Finite Volume Method*". Second Edition.Prentice Hall.
15. Kwang Hyo Jung, Ho Hwan Chun, and Hee Jung Kim. 2008. “Experimental investigation of wing-in-ground effect with a NACA6409 section”. *Journal of Marine Science and Technology* 13 (4): pp. 317-327.
16. “The ANSYS Fluent Adjoint solver getting more from your CFD”. 2013.
17. Athanasios Tzanakis.2014. “Duct optimization using CFD software ‘ANSYS Fluent Adjoint Solver’”. M.S. thesis, Department of Applied Mechanics, Chalmers University Of Technology.